The gas diverges as a fuel mechanism for the active galactic nucleus

Emmanouil Karathanasis,[1]★†
[1]Department of Physics and Mathematics, University of Hull, HU6 7RX, UK

20 September 2023

ABSTRACT

The present study investigates the effect of gas divergence velocity on heating active galactic nuclei (AGN). The results indicate that gas moving negatively inward in a galaxy accumulates at the centre, offering plentiful material for the black hole to accrete and trigger an "active" AGN. On the other hand, in instances where gas diverges at a positive velocity, a substantial proportion moves away from the centre, resulting in the black hole losing its supply of in-falling gas, ultimately causing the AGN to become "dormant". The study involved an analysis of six galaxies, three each from the Illustris-1 and the TNG100-1 simulation. Subsequently, larger data was observed to determine if the model worked effectively across a wider range of galaxies. The aim was to increase our understanding of galaxy formation and evolution and ultimately achieve a grand unification for AGN. The results offer valuable insights into the intricate interplay between gas dynamics and AGN activity in galaxies.

Key words: Active Galactic Nuclei: AGN, Black hole: BH, Galaxy, Simulation, Gas, AGN activity: energy feedback

1 INTRODUCTION

The notion of AGN is of considerable scientific significance. These supermassive black holes (SMBH), situated at the centre of almost every galaxy, significantly impact their surroundings. They generate colossal amounts of energy and rank among the brightest phenomena in the Universe. Seyfert, blazars, radio, and quasars are the four primary classifications of active galaxies. These objects vary in their emission characteristics, specifically concerning the nature of their spectral lines, overall luminosity, and continuum emission at different wavelengths (Jain (2015)). However, a definitive theory of grand unification for AGN activity within the Λ-CDM cosmology does not yet exist due to the considerable differences observed between AGN activity (Fanidakis et al. (2011)). Therefore, a basic model will be utilised based on whether an AGN is "active" or "dormant," depending on the direction of gas flow.

Kawata & Gibson (2003) researched the AGN heating mechanism, aiming to explain the elliptical X-ray and optical features by utilising self-consistent cosmological simulations. Their findings indicated the necessity of a heating mechanism to inhibit enhanced cooling and subsequent star formation in the simulations. In the Kawata & Gibson (2005) explored a feasible mechanism of AGN heating in further research. The objective was to construct precise models of this mechanism and examine the influence of AGN-induced self-regulation on the X-ray and optical characteristics of elliptical galaxies with different luminosities. It is crucial to note that AGN heating effectively resolves the issue of late-time star formation, which was previously identified in the Kawata & Gibson (2003). As a result, Model 2 reliably replicates the X-ray and optical properties of neighbouring ellipticals and establishes a self-consistent heating mechanism for this type of galaxy (Kawata & Gibson (2005)). In this study, the model will be expanded to cover a broader range of galaxies.

The project is focused on constructing a vast data set employing the Illustris simulation (Illustris (2014)). The objective of this research is to determine the direction of gas flow and its correlation to the state of AGNs. The ultimate aim is to create a predictive model that utilises the gas flow direction to ascertain the state of AGNs accurately. Once these predictions have been made, the natural observations will be compared to determine if they accurately predict the number of active AGNs in the Universe or if they over or underestimate them. Despite the challenges faced in this project, it will significantly enhance our comprehension of galaxy formation and evolution.

1.1 Simulations

To satisfy the demands of this hypothesis, the given project aims to compare data originating from two large simulations, the Illustris The Next Generation (IllustrisTNG) and its predecessor, Illustris (Vogelsberger et al. (2014); Genel et al. (2014); Sijacki et al. (2015); Nelson et al. (2015b) Nelson et al. (2019a)). Using these large volumes of cosmological hydrodynamical simulations of galaxy formations will help with data mining and create the appropriate dataset to help the methodological approach to construct a predictive model to determine whether an AGN is active or passive.

Subsequently, both the Illustris and IllustrisTNG simulations are part of the Illustris Project, which aims to comprehend the formation and evolution of galaxies in the visible universe "and to make forecasts for current and forthcoming observational programmes" (Illustris (2014) & TNG (2018)). The IllustrisTNG simulation is the sequel to the original Illustris simulation, with updated and new physics and refinements over the original. The simulations comprise three separate runs (TNG50, TNG100 and TNG300) using the moving-mesh code AREPO and are large-volume, cosmological,

★ E-mail: E.Karathanasis-2015@hull.ac.uk
† E-mail: e.karathanasiss@gmail.com

gravo-magnetohydrodynamical simulations (Springel (2010)). Only TNG100 is utilised for this analysis, with a physical box size denoted by the number: the side lengths of the box for TNG100 are $75Mpc\ h^{-1}\ 106.5Mpc$, where $h = 0.6774$. More specifically, the TNG100-1 run is utilised, consisting of $1820^3 DM$ particles weighing $7.5 \times 10^6\ M_\odot$ and a baryonic mass of $1.4 \times 10^6\ M_\odot$ (Nelson et al. (2015a); Pillepich et al. (2018); Nelson et al. (2019a)).

The study of SMBH evolution and modelling is a critical research field. Weinberger et al. (2018) highlights the prompt identification of friends-of-friends (FoF) groups through dark matter particles. Whenever a FoF halo surpasses a total mass threshold of $7.38 \times 10^10\ M_\odot$ yet lacks an SMBH, an SMBH with a weight of $1.18 \times 10^6\ M_\odot$ is introduced (Nelson et al. (2015a); Pillepich et al. (2018); Nelson et al. (2019a)). As a result, certain low-mass subhalos in dense settings could potentially remain without an SMBH. The subhalos without BHs are not considered. The mass accretion of BHs relies on their immediate surroundings, particularly a Bondi-based recipe that is conditional on the ambient density and sound speed (Kristensen et al. (2021) & Weinberger et al. (2017)). Differing from alternative simulations, the accretion rate is not increased (Springel et al. (2005)). This methodology strengthens the environmental review as it is grounded solely in the physical environment and the processes neighbouring the BH (Kristensen et al. (2021)).

The structures and organisations of both simulations are similar. However, the TNG contains more detailed information than its predecessor, which has recently replaced the Illustris simulations in research studies. To comprehend the data and code, it is necessary first to understand the structure of these simulations. Therefore, Illustris and TNG present three distinct runs. Illustris has Illustris-1, Illustris-2, and Illustris-3, with the first run showcasing a higher resolution and a more significant number of particles (Illustris (2014); Nelson et al. (2015a); Pillepich et al. (2018); Nelson et al. (2019a)). Similarly, TNG has TNG100, TNG300, and TNG50, all of which are high-resolution simulations. However, TNG300-1 has a more significant number of particles than the others. Also noteworthy is that Illustris has three non-dark runs in total, which are runs without dark matter. In contrast, TNG contains ten non-dark runs, with runs ending in one (such as TNG300-1) being the high-resolution runs. Both simulations utilise snapshots that correspond to a specific Redshift (z) (Genel et al. (2013)).

The resolution and particle masses of the two simulations can be compared in Table 1.1 (this table influenced by Kristensen et al. (2021)). However, it is worth noting that TNG100-1 and Illustris-1 have similar box sizes and particle masses. In Illustris, the BH seeds are lighter, but BH accretion is improved in TNG. There are also slight differences in BH feedback mechanisms, which are more thoroughly discussed in Pillepich et al. (2018) and the cited references. Hence, additional runs are used for comparison purposes to verify the validity of the results obtained from TNG100-1 and Illustris-1 (Bhowmick et al. (2020)). Both TNG and Illustris have limitations in their modelling of black holes (Weinberger et al. (2018)). Modern cosmological simulations, such as IllustrisTNG, Horizon-AGN, EAGLE and SIMBA, struggle to produce the diversity of BHs observed in the local Universe (Ward et al. (2022) & Kristensen et al. (2021)). However, we selected galaxies for our AGN based on the galaxy's mass and the black hole's quantity scales with M_{BH} rather than accretion rates (Kristensen et al. (2021)). This lessens the importance of the bias of overmassive SMBHs. Therefore, viewing the results as an objective evaluation of the simulation physics is important. However, to ensure the impact of seed mass was accounted for, the study also includes the Illustris-1 dataset with its lower seed mass compared to the TNG runs.

Simulations	$L_{box}[ckps/h]$	m_{DM}	m_{gas}	m_{BHseed}	Snapshots
Illustris-1	75000	630	130	10/h	136
TNG100-1	75000	750	140	80/h	99

Table 1. Overview of simulation parameters. The first column displays simulation names, whereas the second highlights the corresponding side length in comoving kpc/h. The third column denotes DM particle mass, succeeded by gas cell/particle mass, and seeded BH particle mass. $10^4\ M_\odot$ is used for the masses for simplicity. The final column represents the number of snapshots acquired.

For Illustris, there are 135 snapshots, of which ten are complete, and the first matches to the $z = 46.77$ ($Age_{Gyr} = 0.054$), and TNG has 99 snapshots, of which twenty of them are full snapshots, and the $z = 20.05$ ($Age_{Gyr} = 0.179$) be equivalent to snapshot 0, respectively (Nelson et al. (2015a); Pillepich et al. (2018); Nelson et al. (2019a)). Snapshots contain all particles and cells in the whole volume, which are separated into different groups, "Header", "Parameters", "Configuration", and five "PartTypeX" groups, where data is gathered from the "PartType0" and "PartType5" groups that contain gas particles and BH particles, respectively. Additionally, every snapshot is accompanied by a group catalogue that contains Halos and Subhalos objects. This catalogue is composed of three main components: the "Header," "Group," and "Subhalo" (Nelson et al. (2015a); Pillepich et al. (2018); Nelson et al. (2018)). It is worth noting that the group catalogue does not store the member particle IDs of each group/subhalo in its files. Instead, the particles/cells in the snapshot files are organised based on their group membership. Understanding this distinction is crucial for working with these files effectively.

2 METHODOLOGY

There are three ways to gather data from the simulations. First, the files can be downloaded as raw data to a local system, which is not recommended because, for instance, a snapshot can be 1.5 TB. Secondly, there is an online API that can be used to collect specific galaxies or halos in the form of HDF5 files. Lastly, the Illustris team provides a highly efficient web-based JupyterLab that has been immensely helpful in gathering data (TNG (2018)). This powerful tool has been utilised to investigate and create analysis, execute data-intensive and compute-intensive tasks, and generate final plots for publication. For this project, the latter was chosen to collect and illustrate the data and make the predictive model based on it (Nelson et al. (2015a); Pillepich et al. (2018); Nelson et al. (2018)).

2.1 Galaxies selection

As already stated, AGN is SMBH located at a galaxy's centre. Therefore, a selection was made of each simulation's three most massive centre group galaxies with only one BH at $z = 0$. This choice was made because it was unclear how to find the SMBH in a galaxy with multiple BHs since if a groupcat was made, that finds the subhalo (galaxy) could not separate the overall BH mass. Furthermore, the halo was often mixed with satellite galaxies, making the analysis even more complicated. The Eddington ratio was used to decide the accretion of the chosen BHs. It was assumed that if an SMBH is above fraction $\chi = 1$ (Weinberger et al. (2017) & Ward et al. (2022)),

that means that the given SMBH is in a high-accretion state. Therefore, their Bondi-Hoyle-Lyttleton accretion rate (Bondi (1952); Barai et al. (2014); Bhowmick et al. (2020)) exceeds that of Eddington's accretion rate:

$$\frac{\dot{M}_{Bondi}}{\dot{M}_{Edd}} \geq \chi \tag{1}$$

where

$$\dot{M}_{Bondi} = \frac{4\pi G^2 M_{BH}^2 \rho}{c_s^3} \tag{2}$$

$$\dot{M}_{Edd} = \frac{4\pi G M_{BH} m_p}{\epsilon_r \sigma_\tau c} \tag{3}$$

In which M_{BH} is the BHs mass, G indicates the gravitational constant, c is the speed of light and c_s is the speed of sound (Weinberger et al. (2017) & Nelson et al. (2019b)). The factor ϵ_r is the radiative accretion efficiency, σ_τ the Thompson cross-section, m_p the proton's mass ρ density of the gas near the BHs (Capelo et al. (2023); Barai et al. (2014)). Although, this works for TNG because in the "PartType5", $\dot{M}_{Bondi}$ and $\dot{M}_{Edd}$ are given from the following equations:

$$\dot{M}_{Bondi} = \frac{\alpha 4\pi G^2 M_{BH}^2 \rho}{(c_s^3 + u_{BH}^2)^{\frac{3}{2}}} \tag{4}$$

and $\dot{M}_{Edd}$ are given by form the same equation 3. On the other hand, for Illustris, the Eddington rate (λ) can be defined as:

$$\lambda_{Edd} = \frac{L_{bol}}{L_{Edd}} \tag{5}$$

where

$$L_{bol} = \epsilon_r \dot{M} c^2 \tag{6}$$

$$L_{Edd} = \epsilon_r \dot{M}_{Edd} c^2 \tag{7}$$

Similarly, the Eddington limit is reached with χ when $\lambda_{Edd} = 1$ (Beckman & Shrade (2012) & Ma et al. (2022)), although the Bondi accretion mechanism may not significantly impact AGN fuelling. This assertion is primarily based on the relatively low efficiency of the gravitational potential energy conversion into emergent radiative energy. Consequently, the Eddington limit for most of the selected galaxies was less than one.

2.2 Gas Velocities

The effectiveness of AGN heating seems to correlate with the presence of gas, suggesting that the heating mechanism might only be triggered when nearby gas particles display a negative velocity divergence ($-\nabla \cdot \mathbf{u}$). To determine the velocity field divergence of the neighbouring gas particles, we employed an interpolation technique from the SciPy library (Virtanen et al. (2020)) rather than the SPH scheme used in the relevant research article Kawata & Gibson (2005). Using the griddata technique, the velocity divergence of gas was determined in relation to the BH's position. Two sets of gas data were gathered for every subhalo and halo in the chosen six galaxies, producing two measurements. However, solely the subhalo's velocity divergence was obtained as predictive data owing to the time-intensive code processing, taking over twelve hours. This dataset computed the typical velocity divergence to streamline the outcomes. Additionally, for comparison purposes, the divergence of gas velocity and its radial velocity were computed exclusively for the galaxy (Crenshaw et al. (2010) & Nelson et al. (2019b)). Furthermore, for simplicity, the mean results of the velocities are presented.

2.3 Luminosity and Feedback

An analysis that produced two different luminosities for a BH was carried out as part of a research project. To determine the bolometric luminosity of the BH, the following equation 6 was used. In this equation, L_{bol} is the bolometric luminosity of the BH, while $\dot{M}$ is the accretion rate of mass to the BH. In addition, the Eddington luminosity is the maximum luminosity that can be reached by the BH and is denoted by L_{Edd} in equation 7. Both luminosities were used in the early analysis; however, only the bolometric luminosity (L_{bol}) was used in the dataset prepared for the predictive model.

As previously mentioned, the AGN is considered active when the energy feedback reaches $10^{44} ergs^{-1}$ (Kawata & Gibson (2005)). However, the nature of its activity varies depending on whether the accretion is low or high. Hence, the equation for the low accreting energy feedback (thermal energy) is given by:

$$\Delta \dot{E}_{low} = \epsilon_{f,kin} \dot{M}_{BH} c^2 \tag{8}$$

where $\epsilon_{f,kin}$ for low-accretion BH is 0.2 (Weinberger et al. (2017)). For high-accretion rate BH, the energy feedback is given by the following equation:

$$\Delta \dot{E}_{high} = \epsilon_f \epsilon_r \dot{M}_{BH} c^2 \tag{9}$$

Where ϵ_f is the coupling efficiency in the high-accretion state at the constant value of 0.1 and ϵ_r is the radiative efficiency (Weinberger et al. (2017)). In the initial analysis of Illustris, we used equation 9 (Ma et al. (2022)). However, due to the lower radiative efficiency value from the TNG simulation, the thermal feedback was consistently low, preventing AGN activity. The equation 8 was employed for TNG galaxies, as they were in a low-accretion state. Finally, equation 8 was used because the data for the prediction model were only obtained from the TNG.

2.4 Additional Data and Morphology

For this study, further data has been collated to analyse the six galaxies. The mass of the BH was measured to track its growth over time for all six galaxies. In addition, the subhalo group was used to obtain the star formation rate (SFR) instead of "PartType4", which contains the data on stars and winds (Nelson et al. (2015a); Pillepich et al. (2018); Nelson et al. (2019a)). This resulted in the SFR of the entire galaxy being obtained rather than just a specific part of it. Additional data has also been acquired for the three TNG galaxies. For instance, the "BH CumEgyInjection QM" from "PartType5" represents the amount of thermal AGN feedback energy injected into surrounding gas during the high accretion-state (quasar) mode, summed over the entire lifetime of this BH field calculated during the BH-BH merger (TNG (2018); Nelson et al. (2015a); Pillepich et al. (2018); Nelson et al. (2019a)). Also, from the same field, the "BH CumEgyInjection RM" represents the total mass accumulated onto the BH during its high accretion-state (quasar) mode throughout its lifetime. This value is summed over the entire field during the merger of two black holes (TNG (2018); Nelson et al. (2015a); Pillepich et al. (2018); Nelson et al. (2019a)).

The morphology of the six galaxies differs, as inferred from the SKIRT Synthetic Images (Illustris (2014) & TNG (2018)). The "broadband sdss.fits" (Stoughton et al. (2002)) were collected individually to determine their morphology. Beginning with the TNG

galaxies, with id = *356678* based on the Conselice (2003), the asymmetry of the galaxy is close to a merging process $a = 0.33$ and the concentration is closer to a spiral galaxy (Lotz et al. (2004), Peth et al. (2016)). For id = *359811*, the concentration and asymmetry suggest a similarity to a spiral galaxy. However, id = *408764* appears to be an elliptical galaxy, characterised by high concentration and a lack of asymmetry (Peth et al. (2016)). Additionally, the Illustris galaxies (id = *305959*, id = *321859*, and id = *347122*) demonstrate high concentration values of $C > 3$, with asymmetry levels similar to that of id = *408764* from TNG. The morphology was identified using the *statmorph* code in TNG (2018). It was created based on the knowledge in Conselice (2003), Lotz et al. (2004), and Peth et al. (2016), as well as from Rodriguez-Gomez et al. (2019), which created the code. Also, the gas distribution and temperature in six galaxies are shown in the following plots (see Appendix A1). The galaxies from Illustris can be obtained using the API code provided in the example by Illustris (2014), which are depicted in the images below (see Appendix A2).

For the prediction's conclusive data, supplementary data was added to observe the correlation to the AGN's activity. The SFR in half a rad was extracted similarly as previously performed on the galaxies but with limitations to cells within the stellar half-mass radius. In addition to the above information, the metallicity of a galaxy's SFR was included, represented by the mass-weighted mean metallicity ($\frac{Mz}{Mtot}$, where Z equals any element above He) of gas cells bound to the respective Subhalo. However, this calculation excludes cells that are not involved in star formation. Additionally, the U-band was obtained from stellar photometric measurements of the Subhalo (Donnari et al. (2019)). Although, the velocity dispersion data was omitted as it remained constant throughout the redshift (z). It is unclear what the morphology of the 30,000 galaxies is because of the vast amount of galaxies from different redshifts.

3 RESULTS AND DISCUSSION

To progress to the results, further information is necessary. The selected galaxies analysed have undergone major and minor mergers, outlined in table 3. However, the number of mergers is known, and their occurrence, which redshifts, is uncertain (Genel et al. (2013); Srisawat et al. (2013); Rodriguez-Gomez et al. (2015)). As a result, the connection between SFR and mergers cannot be established. As shown in the diagram 1, the Illustris galaxies exhibit spikes in their SFR, which may result from mergers. In contrast, the TNG galaxies do not display any spikes, with the galaxy $id = 408764$ appearing to be a quenched galaxy, where the SFR has been suppressed for a long time. Furthermore, $id = 356678$ shows a continuous reduction in SFR, which reaches zero at a redshift of 0.4. On the other hand, $id = 359811$ experiences a sharp decline in SFR until it reaches zero at a redshift of 2. The reason for such a sudden decrease in SFR remains unknown. Overall, it appears that the galaxies in TNG have undergone more major mergers than their counterparts in SFR, which could potentially explain the early decay of their SFRs.

3.1 Results

During the initial phase of the analysis, it is evident from figure A3 that all six galaxies' BHs increased in mass, with predominantly constant growth. However, some BHs exhibited a significant increase, including the TNG galaxy with the identifier $id = 356678$, which underwent a swift rise in BH mass from $z = 3$ to $z = 1.5$, followed by a steady but slight expansion until $z = 0$. Similar to TNG *356678*, all of the Illustris galaxies and TNG's specific galaxy *359811* display

Galaxy ID	num Major Mergers	num Minor Mergers
Ill 305959	3	2
Ill 321863	1	7
Ill 347122	3	4
TNG 356678	3	4
TNG 359811	4	2
TNG 408764	6	2

Table 2. The number of major and minor mergers that galaxies have undergone in the past.

similar peaks. However, the TNG galaxy with $id = 408764$ has experienced the smallest growth over time, which can be attributed to its zero SFR. As shown in Figures A4 and A5, the top panel illustrates the AGN activity over redshift, provided by the energy feedback injected from the BH. The dashed line indicates when the log of energy feedback exceeds *44*, indicating AGN activity. TNG galaxies (see appendix A4) were active at $z = 2.5$, followed by only galaxy *356678* until close to $z = 1$, after which their AGN remained inactive. It was clearly demonstrated to the other panels in the initial activity of the AGN that velocities were predominantly negative. However, the divergence of the gas on the Halo showed a positive trend for most galaxies. In particular, when divergences were negative for galaxy *356678*, the energy feedback exceeded the threshold. Moreover, the AGN for this specific galaxy became inactive when gas velocities approached zero.

Conversely, the Illustris galaxies (refer to appendix A5) were active twice, except for galaxy $ID = 321863$, which was almost active but remained in a dormant state due to our current lower limit for energy Feedback. Additionally, the other two galaxies initially exhibited activity twice, which initially bolstered the argument; however, as demonstrated in all three panels below the top panel, they ultimately did not support it. The velocities tended to be positive, particularly in the case of V_{rad}. Another notable observation was that the divergence between the gas of the whole galaxy and the Halo was not that different, especially in Illustris. However, on TNG excepted the *356678* galaxy, in which the divergences are similar. Initially, the other two galaxies have varying values, but eventually, they tend to have similar values, as seen at $z = 0.8$ for *359811* and $z = 0.5$ for *408764*. Even though their values differ initially, the two divergences follow a similar direction.

To further analyse the theory and assess its validity, predictive data was extracted from 30,000 galaxies in the TNG simulation using predictive modelling. The energy feedback of these galaxies is displayed in figure B1, demonstrating that the majority of them are currently inactive. The threshold represents the energy feedback required for BH to be considered active. The predictive data aim to develop a machine-learning model that accurately predicts the AGN's activity by analysing the gas divergence velocity and radial velocity. The results in figures B2 and B3 demonstrate the correlation between velocities and each AGN's activity across various redshifts containing 10,000 galaxies. Dormant galaxies are prevalent in negative and positive velocities, contradicting our theory. The utilisation of machine learning models revealed that the logistic regression classifier yielded the highest accuracy of 83.15% when utilising the observed velocities, with the divergence velocity ranking as the most significant model feature slightly ahead of the radial velocity. Additionally, imbalance classifiers were implemented, where the highest accuracy achieved was 66.7%. Therefore, the $\dot{M}_{BH}$ was incorporated into the model, resulting in an improvement of accuracy to 98.26%. Logistic regression and the decision tree classifier achieved this level of ac-

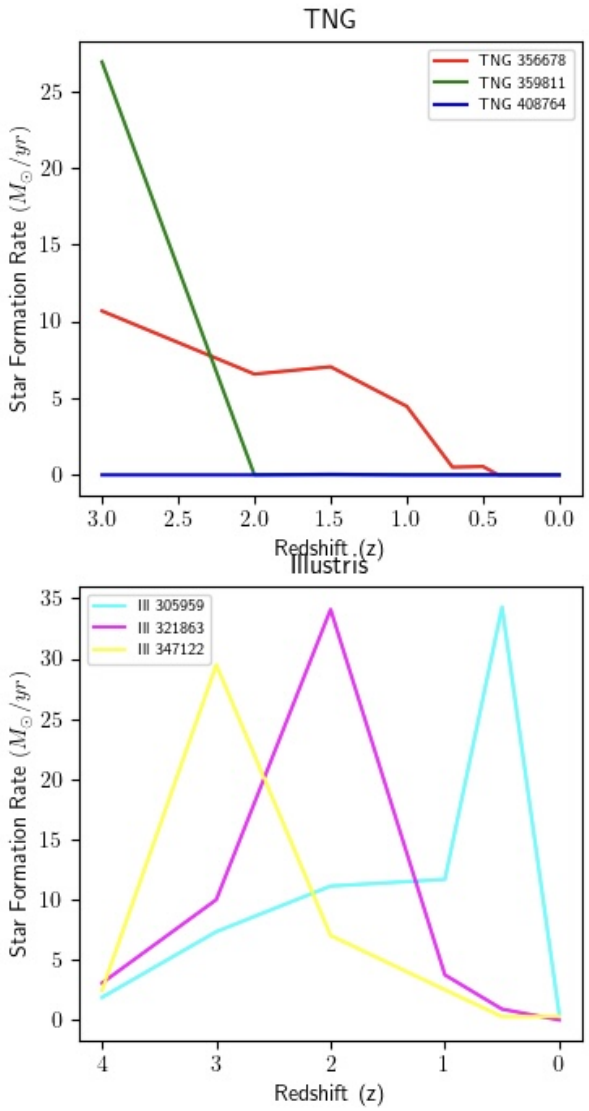

Figure 1. The figure shows the star formation rate ($\frac{M_\odot}{yr}$) versus redshift z for each galaxy selected for analysis. At the top are the TNG galaxies at the bottom are the Illustris galaxies.

curacy, whereas the neural network exhibited over-fitting due to the simplicity of the data.

3.2 Discussion and Other Studies

The TNG's preliminary analysis reveals some degree of concurrence with the theory, but the Illustris galaxies highlight that the sample does not validate it. Since TNG provides more detailed information through fuller and closer snapshots, it surpasses Illustris, which lacks detail in comparison. For instance, TNG presents ten full snapshots from $z = 0$ to $z = 2$, whereas Illustris only has three. Primarily, the data for the predictive model was collected exclusively from TNG100-1 for this reason. However, during the final analysis, this model was found to be inadequate to prove the theory's effectiveness. Instead, it demonstrated that the theory is ineffective and that further characteristics must be considered to determine whether the gas's divergence activates AGN. Two new questions have emerged from this study: firstly, how would the merging of galaxies impact the SMBH if it merged with other BHs, potentially indicating that the AGN became active? Secondly, considering that the model's accuracy increased due to the $\dot{M}_{BH}$, the primary cause of an AGN, the question arises regarding how much of the divergent cold gas reaches the SMBH to be accreted.

Other studies have revealed a correlation between AGN obscuration and galaxy mergers, confirming the established perception that mergers can stimulate material inflow into the inner tens of parsecs (Ricci et al. (2017)). Additionally, the proximity of AGN within late-merging galaxies is found to be more abundant in gas and dust than AGN in solitary galaxies (Ricci et al. (2017)). However, this study proposes that, for the past 7.5 Gyr, the primary trigger for typical AGNs has not been the major merging. Instead, minor interactions and internal secular processes have been responsible for the majority of BH accretion (Cisternas et al. (2011)). Moreover, the velocity of CO(2-1) measurement indicates a slight connection between the molecular gas fraction and the Eddington ratio of the host galaxy, potentially linked to gravitational instability or rapid cold gas inflow igniting nuclear starbursts and feeding the BHs (Molina et al. (2023)). There is also a faint correlation present between the AGN's CO(2–1) line luminosity and the molecular gas fraction and Eddington ratio of the host galaxy (Molina et al. (2023)). Though, this association disappears when considering the evolution of gas content in galaxies across the universe. AGN hosts with higher luminosity appear at greater redshifts, suggesting a lack of correlation between AGN luminosity and the total molecular gas content of their host galaxy (Molina et al. (2023)). The second correlation infers that the gravitational instability of the host galaxy or the rapid inflow of cold gas induces AGN activity. These results indicate that negative feedback from AGNs is ineffective (Molina et al. (2023)).

4 CONCLUSIONS

In conclusion, the study aimed to establish whether the activity of the AGN is solely affected by the divergence velocity of the gas across the galaxy. The use of Illustris-1 and TNG100-1 simulations showcased evidence supporting this theory through the analysis of divergence and radial velocities in the early stages. The findings witnessed a correlation between the velocities and the energy feedback introduced by the AGN. However, the analysis revealed that additional features must be considered, like $\dot{M}_{BH}$ and the merges. Additionally, there is no complete grand unification of AGN activity within the Λ-CDM cosmology theory, leading to gaps in older theories and methodologies. Therefore, this study requires further investigations to complete the hypothesis. Ultimately, it was demonstrated that the divergence and radial velocities of the gas alone are insufficient for predicting AGN activity. Nevertheless, its crucial importance, our comprehension of AGNs remains incomplete, and researchers require a more complete view, necessitating additional research.

ACKNOWLEDGEMENTS

I would like to thank the invaluable support and guidance of Dr. K. Pimbblet, without whom this Master's project would not have been possible, especially in these challenging times; Professor B. Gibson for giving me the opportunity to explore such a fascinating topic; and I would also like to thank Dr. N. Dylan, a member of the Illustris project team, for providing me with access to JupyterLab, which allowed me to carry out my research.

REFERENCES

Barai P., Viel M., Murante G., Gaspari M., Borgani S., 2014, Monthly Notices of the Royal Astronomical Society, 437, 1456

Beckman V., Shrade C., 2012, Active Galactic Nuclei, 1st edn. WILEY-VCH

Bhowmick A. K., Blecha L., Thomas J., 2020, The Astrophysical Journal, 904, 150

Bondi H., 1952, Monthly Notices of the Royal Astronomical Society, 112, 195

Capelo P. R., Feruglio C., Hickox R. C., Tombesi F., 2023, Black Hole-Galaxy Co-evolution and the Role of Feedback. Springer Nature Singapore, pp 1–50, doi:10.1007/978-981-16-4544-0_115-1

Cisternas M., et al., 2011, The Astrophysical Journal, 726, 57

Conselice C. J., 2003, The Astrophysical Journal Supplement Series, 147, 1

Crenshaw D. M., Schmitt H. R., Kraemer S. B., Mushotzky R. F., Dunn J. P., 2010, The Astrophysical Journal, 708, 419

Donnari M., et al., 2019, Monthly Notices of the Royal Astronomical Society, 485, 4817

Fanidakis N., Baugh C. M., Benson A. J., Bower R. G., Cole S., Done C., Frenk C. S., 2011, Monthly Notices of the Royal Astronomical Society, 410, 53

Genel S., Vogelsberger M., Nelson D., Sijacki D., Springel V., Hernquist L., 2013, Monthly Notices of the Royal Astronomical Society, 435, 1426

Genel S., et al., 2014, Monthly Notices of the Royal Astronomical Society, 445, 175

Illustris C., 2014, The Illustris Simulation, https://www.illustris-project.org

Jain P., 2015, An introduction to astronomy and astrophysics, 1st edn. CRC Press

Kawata D., Gibson B. K., 2003, Monthly Notices of the Royal Astronomical Society, 346, 135

Kawata D., Gibson B. K., 2005, Monthly Notices of the Royal Astronomical Society: Letters, 358

Kristensen M. T., Pimbblet K. A., Gibson B. K., Penny S. J., Koudmani S., 2021, The Astrophysical Journal, 922, 127

Lotz J. M., Primack J., Madau P., 2004, The Astronomical Journal, 128, 163

Ma W., Liu K., Guo H., Cui W., Jones M. G., Wang J., Zhang L., Davé R., 2022, The Astrophysical Journal, 941, 205

Molina J., Shangguan J., Wang R., Ho L. C., Bauer F. E., Treister E., 2023, The Astrophysical Journal, 950, 60

Nelson D., et al., 2015a, Astronomy and Computing, 13, 12

Nelson D., Genel S., Vogelsberger M., Springel V., Sijacki D., Torrey P., Hernquist L., 2015b, Monthly Notices of the Royal Astronomical Society, 448, 59

Nelson D., et al., 2018, Monthly Notices of the Royal Astronomical Society, 475, 624

Nelson D., et al., 2019a, Computational Astrophysics and Cosmology, 6, 2

Nelson D., et al., 2019b, Monthly Notices of the Royal Astronomical Society, 490, 3234

Peth M. A., et al., 2016, Monthly Notices of the Royal Astronomical Society, 458, 963

Pillepich A., et al., 2018, Monthly Notices of the Royal Astronomical Society, 473, 4077

Ricci C., et al., 2017, Monthly Notices of the Royal Astronomical Society, p. stx173

Rodriguez-Gomez V., et al., 2015, Monthly Notices of the Royal Astronomical Society, 449, 49

Rodriguez-Gomez V., et al., 2019, Monthly Notices of the Royal Astronomical Society, 483, 4140

Sijacki D., Vogelsberger M., Genel S., Springel V., Torrey P., Snyder G. F., Nelson D., Hernquist L., 2015, Monthly Notices of the Royal Astronomical Society, 452, 575

Springel V., 2010, Monthly Notices of the Royal Astronomical Society, 401, 791

Springel V., et al., 2005, Nature, 435, 629

Srisawat C., et al., 2013, Monthly Notices of the Royal Astronomical Society, 436, 150

Stoughton C., et al., 2002, The Astronomical Journal, 123, 485

TNG C., 2018, The IllustrisTNG Project, https://www.tng-project.org

Virtanen P., et al., 2020, Nature Methods, 17, 261

Vogelsberger M., et al., 2014, Nature, 509, 177

Ward S. R., Harrison C. M., Costa T., Mainieri V., 2022, Monthly Notices of the Royal Astronomical Society, 514, 2936

Weinberger R., et al., 2017, Monthly Notices of the Royal Astronomical Society, 465, 3291

Weinberger R., et al., 2018, Monthly Notices of the Royal Astronomical Society, 479, 4056

APPENDIX A: ANALYSES RESULTS

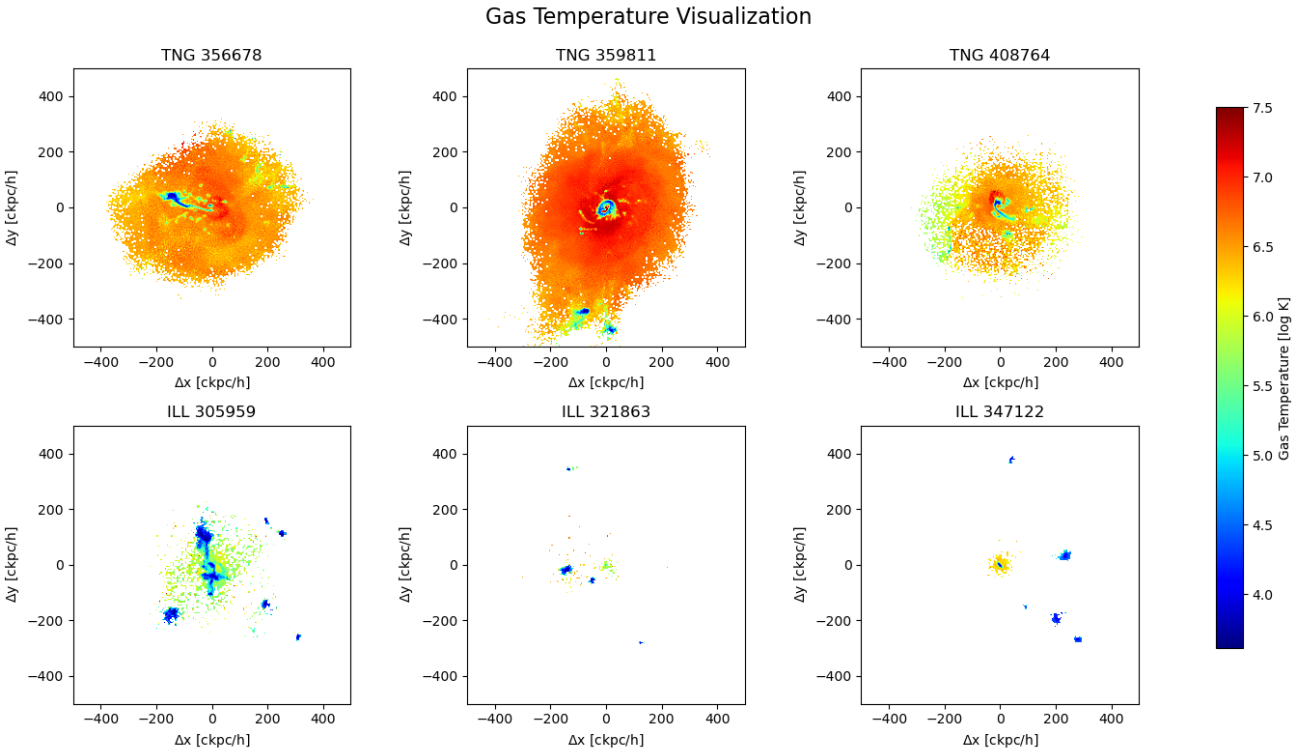

Figure A1. The figure illustrates the gas temperature distribution in the six galaxies selected for analysis. The three galaxies positioned at the highest point are TNG simulations, denser and more intricate than the three galaxies below, which come from the Illustris simulation. Note that the pixels used in the Illustris galaxies were larger than those used in TNG.

Figure A2. These three images depict galaxies from the Illustris Project obtained through the method outlined at the end of the API section.

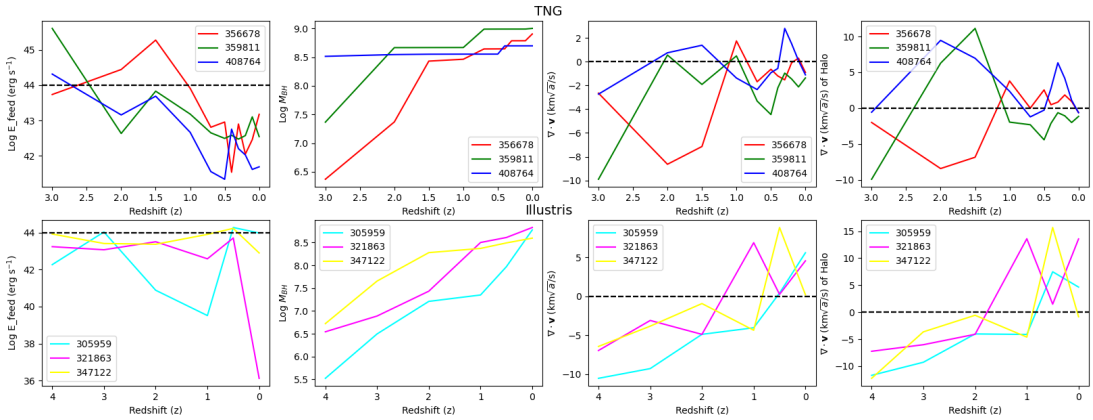

Figure A3. These graphs present a comparison of TNG and Illustris galaxies. The left-hand graphs depict the AGN activity. The subsequent pair of graphs exhibit the increase in BH mass. The last four graphs demonstrate the average divergence velocity of the gas, where the first represents the entire galaxies and the remaining two show the corresponding halos.

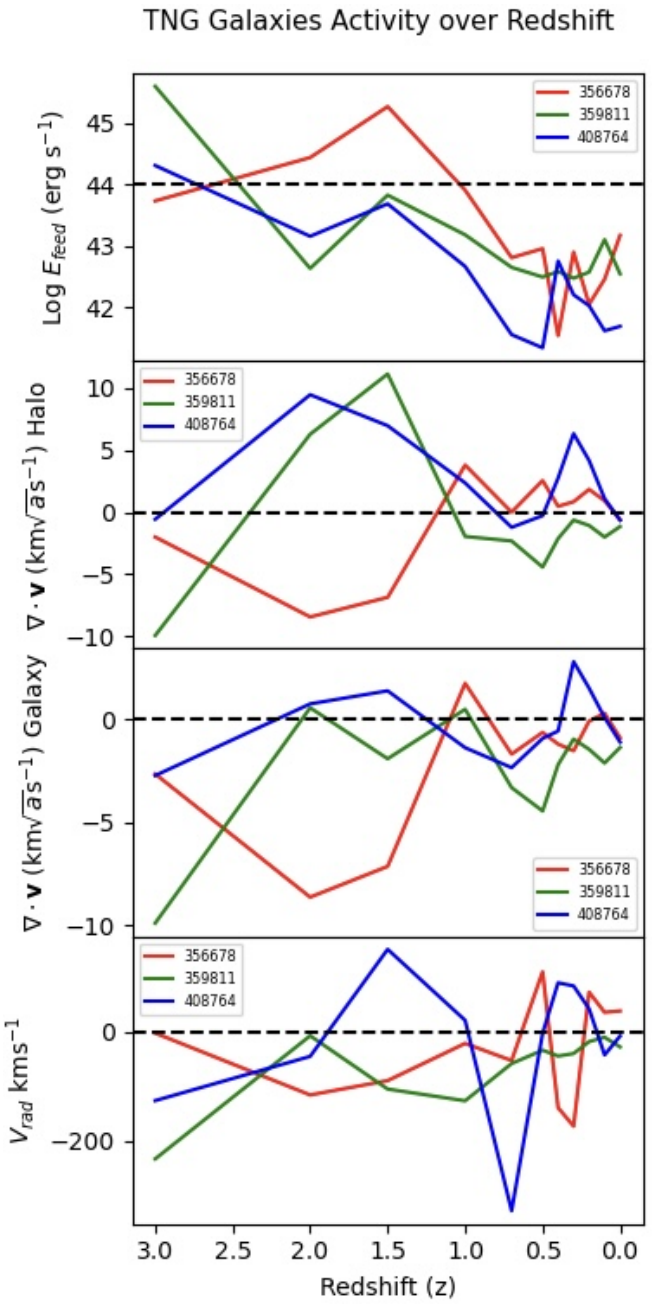

Figure A4. This figure depicts the redshift-dependence of AGN activity in TNG galaxies. The top panel presents the base-10 logarithm of energy feedback. An active AGN is represented by energy passing the black dashed line. The middle panels shows the average divergence of gas in the halo and in the galaxy. The dashed line demarcates positive and negative divergence. Similarly, the lower graph displays the mean radial velocity of the gas across the entire galaxy, with the dotted line demarcating the positive and negative velocity.

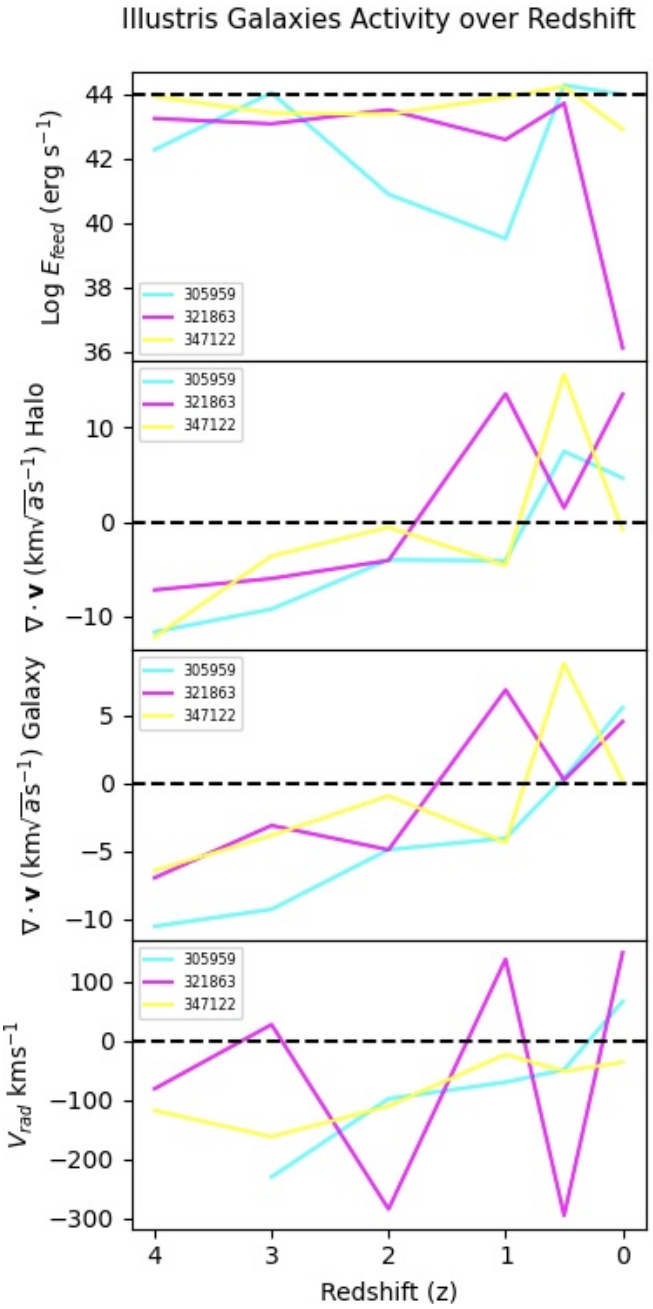

Figure A5. This plot shows the AGN activity versus redshift for the Illustris galaxies. At the top is the log_{10} of the energy feedback and the black dashed line indicates that when the energy passes this line the AGN is active. The two middle plots shows the average divergence of the gas in the halo and in the galaxy, and the dashed line has been used to separate the positive divergence from the negative. Similarly, the bottom plot shows the average radial velocity of the gas in the whole galaxy and the dashed line is used to separate the positive from the negative velocity.

APPENDIX B: DATA PREDICTION FIGURES

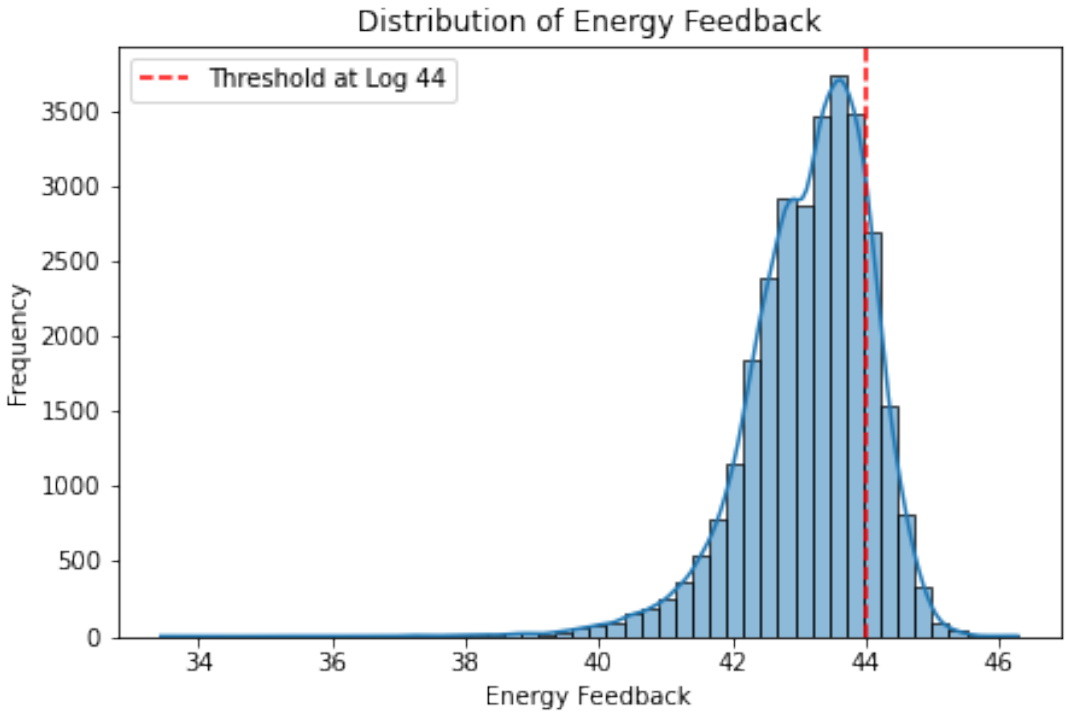

Figure B1. The following graphs illustrate the distribution of Energy Feedback in the predictive data. Galaxies that are at or above the specified threshold are considered to have active AGN, while those below it are considered to have dormant AGN.

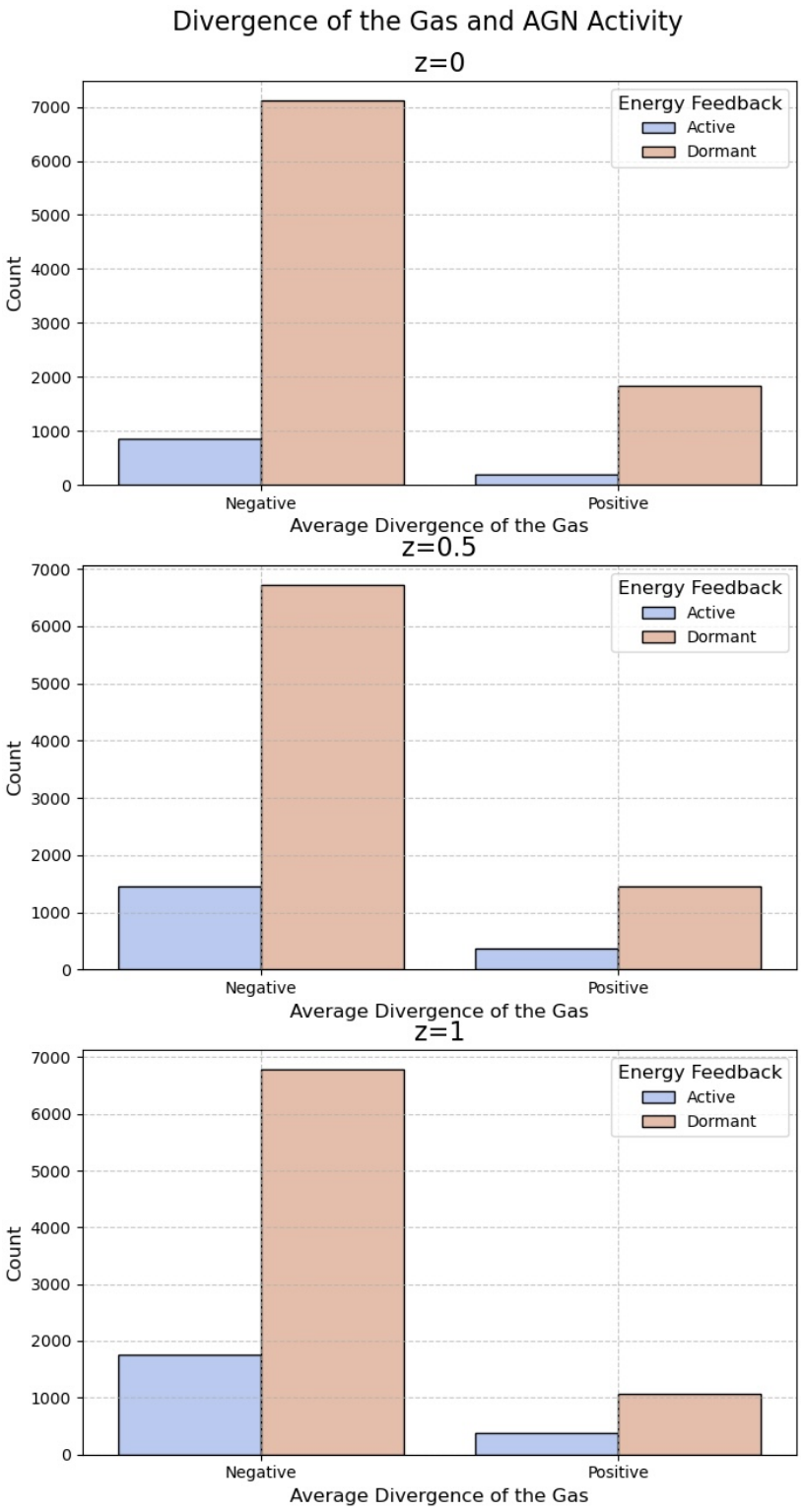

Figure B2. These charts display the average divergence of the gas at three distinct redshifts and AGN activity. It indicates that if the energy feedback of the AGN is equal to or above $log_{10}44$, then the AGN is active when negative or positive average divergence velocity exists. When the velocity is below this value, however, the AGN is passive.

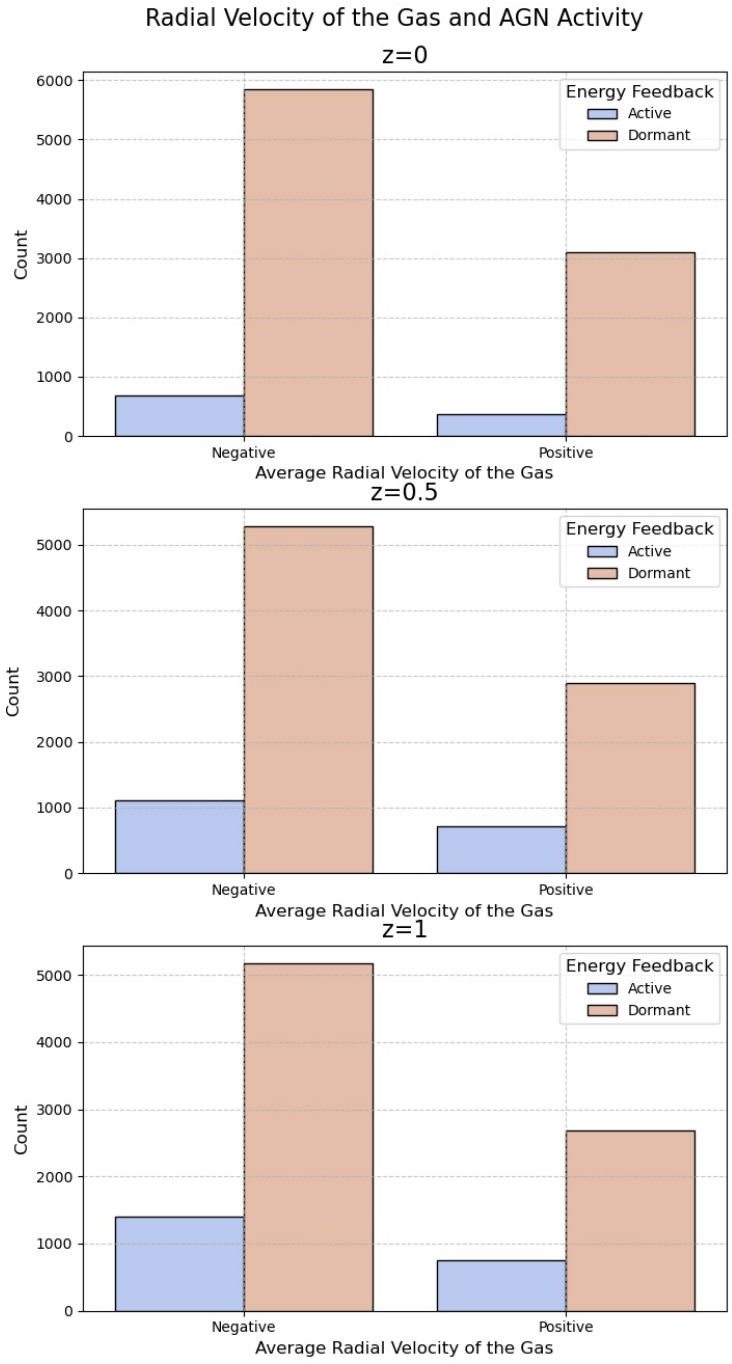

Figure B3. These charts depict the mean radial velocity of the gas at three different redshifts and levels of AGN activity. It suggests that an active AGN will present negative or positive mean radial velocity if its energy feedback is at or above $log_{10}44$, whereas if the velocity falls below this value, it is passive.

This paper has been typeset from a TEX/LATEX file prepared by the author.